Materials Today: Proceedings xxx (xxxx) xxx

Contents lists available at ScienceDirect

Materials Today: Proceedings

journal homepage: www.elsevier.com/locate/matpr

Numerical investigation on stress intensity around Bone-Implant interface by 3-Dimensional FEA and experimental verification by optical technique

Pankaj Dhatrak [a,*], Uddhav Shirsat [b], S. Sumanth [c], Vijay Deshmukh [d]

[a] School of Mechanical Engineering, Dr. Vishwanath Karad, MIT-WPU (Formerly MAEER'S MIT) Pune 38, India
[b] Department of Mechanical Engineering, Bhivarabai Swanat College of Engineering & Researach, Pune 41, India
[c] Department of Periodontic, M. A. Rangoonwal College of Dental Science and Research Centre, Pune 01, India
[d] International Clinical Dental Research Organisation, Pune 38, India

ARTICLE INFO

Article history:
Received 24 March 2020
Received in revised form 19 May 2020
Accepted 6 June 2020
Available online xxxx

Keywords:
Cancellous bone
Dental Implant
FEA
Optical Technique
Photoelastic stress

ABSTRACT

The aim of the current study is to examine numerically the stress intensity along bone-implant interface for selected implant systems under occlusal load using finite element analysis (FEA) and confirming the result experimentally by optical technique. To see the biomechanical performance at bone-implant interface the five types of implant systems are chosen for the current study. A three-dimensional (3D) computer aided design (CAD) is prepared using CreO Parametric modeling software. A non-linear contact between implant and surrounding bone is defined to analyze the stress intensity in the cancellous bone under the applied load of 100 N axial directions, 40 N laterals (Bucco-lingual) direction and 100 N oblique at 45 degree to the longitudinal axis of implant. An experimental photoelastic technique (Optical technique) is used to predict the stress intensity in a cancellous bone near the bone-implant interface using Tardy's method of compensation. A homogeneous blend of Araldite and hardener material is used to prepare a photoelastic block model. The maximum value of stress intensity is noted in Type-I implant system at apical part of implant whereas minimum value was noted in Type-III implant system under lateral and oblique loads. Stress intensity in cancellous bone at the bone interface is found to be more significant to the applied oblique load.

1. Introduction

Nowadays pure titanium and titanium alloy based dental implants in the edentulous mandible are widely used as an artificial tooth in place of damaged or missing natural tooth [1]. The biomechanical compatibility between bone and implant is achieved with certain bonding between them commonly known as osseointegration [2]. Different factors influence osseointegration like implant thread design, bone quality, clinical techniques and postoperative treatment. Among these factors, implant design is one of the dominant factors. In addition, implant thread profile is directly affected the stress pattern to the adjacent bone and marginal bone loss [2–4]. Different sizes and shapes of implant thread profile are available commercially. It is essential to understand the effect of thread profile on stress distribution to the surrounding bone for the rehabilitation success [5]. A five commercially available implant systems (selected based on the literature review) are numerically and experimentally investigated to analyze the stress intensity in a cancellous (jaw) bone to understand the biomechanical behavior of implant (thread profile) with surrounding bone. In order to study the stress pattern, a molar region of mandibular section (Type-II bone -dense cancellous bone surrounding with 2 mm thick cortical) with reference toLekholm and Zarb classification [6] is modelled and the stress intensity around the bone interface is numerically evaluated by finite element method using ABAQUS6.10.3 simulation code.

2. Dental implant system

Various implant design might affect the type and magnitude of force applied to the bone-implant interface. Five commercially

* Corresponding author.
E-mail address: pankaj.dhatrak@mitwpu.edu.in (P. Dhatrak).

https://doi.org/10.1016/j.matpr.2020.06.097
2214-7853/

available dental implant system with internal hex connection are selected. Implant system (Type-I) (3.5 mm diameter, 14 mm length), Implant system (Type-II) (3.4 mm diameter, 15 mm length), Implant system (Type-III) (3.5 mm diameter, 14 mm length), Implant system (Type-IV) (3.5 mm diameter, 15 mm length) and Implant system (Type-V) (3.5 mm diameter, 15 mm length). Small variation in implant diameters and length was predictable since most of the manufacturers do not support implants with similar sizes.

3. Materials and methodology

3.1. 3D-CAD geometry modeling

The implant dimensions like diameter and length were presented from manufacturer catalogue and other parameters like pitch, thread profile, thread depth, thread height, number of turns were measured using video Measuring system (Vision Engineering, make: SWIFT DUO, UK). The geometric 3D CAD models of the five implants are represented in Fig. 1. The complete implant prosthesis (implant, crown, abutment, and intermediate screw and jawbone) assembled in CAD software. The CAD assembly model is imported in HYPERMESM software for finite element (FE) modeling.

3.2. 3D FE modeling

3.2.1. Convergence Criteria

In the present study the mesh refinement was performed to satisfy the convergence criteria. The equivalent stress in the cancellous and cortical bone were monitored to obtain the desired convergence in the implant prosthetic assembly. Based on variation in the mesh size, the change in the jawbone model is observed. If the variation is less than 5% then, it was considered as a mesh convergent [4, 7, and 8].

3.2.2. Nodes and Elements

The implant, abutment, intermediate screw and bone have been meshed with C3D10 quadratic tetrahedron element with average size of 0.08 mm whereas the crown has been modeled with S3R/S4R linear tri/quadrilateral element with average size of 0.3 mm. Different mesh refinement levels were used to control the model size for numerical solution [7,8]. The bone-implant interface region is fine meshed to accurately model the thread profile and the cancellous and cortical region away from interface is coarse meshed to control the size of FE model shown in Fig. 2 (b). The total number of nodes and elements in all five-implant system is shown in Table 1.

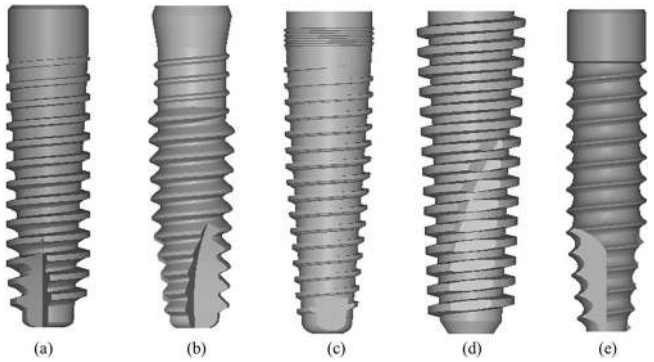

Fig. 1. 3D CAD Model of implant system Type-I to Type V (a-e).

3.2.3. Implant and bone Interface

The bio-mechanical properties of implant and bone interface are defined by the size of implant surface in contact with tissue around the interface. Therefore, it is a key factor for implant stability [9]. A friction contact is defined to simulate the bone-implant interface condition [10,11]. The bone-implant interface is modeled as surface contact and the friction coefficient is 0.3 with small sliding to simulate ideal osseoinegration in FE simulation.

3.2.4. Material Properties

A pure Titanium and Titanium alloy widely acceptable as an implant material in the field of dentistry because of its good biocompatible and mechanical properties. The material with isotropic properties was developed by most of the researchers which consists of giving material properties, prominent boundary conditions and performing the mesh model with numerical simulation. Some of the investigators assumed bone anisotropy is a complex orthotropy [12]. The material model with orthotropic properties was prepared by giving properties in a random direction and then solving for vertical, lateral and oblique loads requirement in order to characterize the final control of axes of orthotropy. With these directions specified to each element, a final result was achieved [13,14]. Local alignment of the orthotropic material along the bone structure is established on direction of principle stresses formed by masticatory loading and distinct boundary conditions. The nonlinear elastic properties of implant prosthetic were assumed in this study shown in Table 2.

3.2.5. Load and constraints

Vertical and lateral forces mainly induce due to mastication and horizontal motion of the mandible [15]. Three loading conditions were simulated in FE simulation [8,16–18]. A vertical 100 N load (mastication force) in coronal to apical direction, lateral load (transverse force due to motion of mandible & inclination of tooth cusps) of 40 N in Bucco-lingual direction (cheek-tongue direction) and the 100 N oblique load at 45° inclination with axis of implant were used to analyze the stress distribution in the cancellous bone in the vicinity of bone interface. The oblique load is resolved into two components as a vertical and horizontal component of forces on the crown surface. In FEA to represent the physical boundary condition of holding the acrylic block model is simulated by constraining the nodes in all DOF. The bottom 1/3rd portion of block model nodes from all sides were constraints to zero DOF. A nonlinear contact stress analysis was performed using Abaqus/CAE code. 3D finite element model (FEM) with loads and constraints are shown in Fig. 2(c)

4. Experimental work

4.1. Photoelastic test setup

An experimental photoelastic method generally used for stress analysis of complicated geometry with vertical loading conditions [19]. Photoelastic test setup involves of a light supply, polarizer and analyzer plates, loading fixture and a load cell as demonstrated in Fig. 3 (a). Isochromatic pattern of fringes under specified loading were observed in monochromatic light as shown in Fig. 3 (c). A magnifying lens is accessible for accelerating measurement of fringes. Tardy's method of compensation was used to evaluate isochromatic fringes [20].

4.2. Photoelastic material model

Experimental photoelastic block model is approximated to a cuboid shape of dimensions 10 mm (thickness) × 20 mm

Please cite this article as: P. Dhatrak, U. Shirsat, S. Sumanth et al., Numerical investigation on stress intensity around Bone-Implant interface by 3-Dimensional FEA and experimental verification by optical technique, Materials Today: Proceedings, https://doi.org/10.1016/j.matpr.2020.06.097

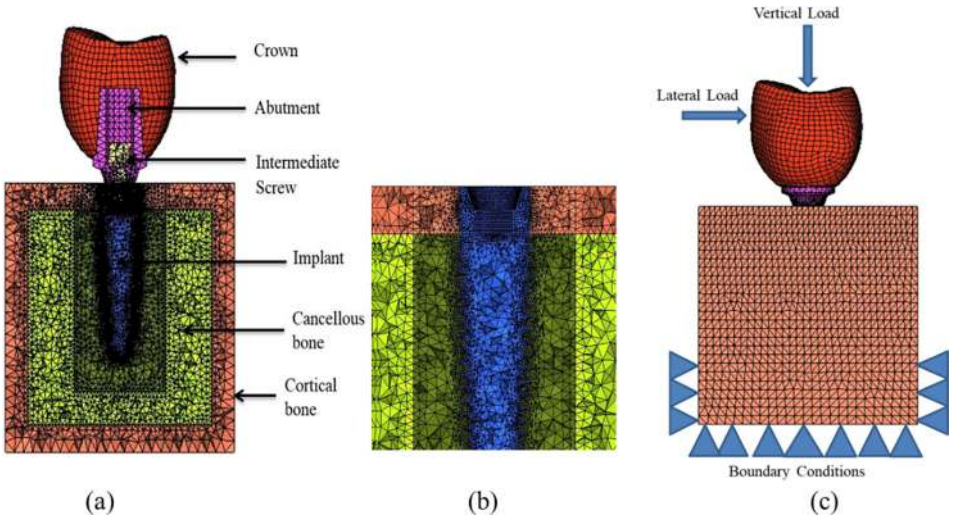

Fig. 2. FE model of implant system (a) Cut section of 3D FE model of implant-bone assembly, (b) Mesh enhancement at bone-implant interface (c) loads and boundary condition employed on implant system.

Table 1
Number of nodes and elements in the Implant System.

Implant System	Elements	Nodes
Type-I	671,924	144,601
Type-II	837,510	167,502
Type-III	783,975	158,528
Type-IV	847,519	177,752
Type-V	770,007	153,365

Table 2
Orthotropic properties of jawbone applied in FE Model [12].

Sr. No.	Material Properties	Cancellous bone	Cortical bone	
1	Elastic Moduli (MPa)	E1	210	12,700
		E2	1148	17,900
		E3	1148	22,800
2	Shear Moduli (MPa)	G12	68	5000
		G13	68	5500
		G23	434	7400
3	Poisson's ratio	μ12	0.055	0.18
		μ21	0.105	0.35
		μ13	0.055	0.31
		μ31	0.093	0.49
		μ23	0.322	0.28
		μ32	0.325	0.31

(width) × 25 mm (height), since maximum load is always concentrated in the small zone around the neck region of implant and surrounding bone, therefore the shape of the cut section of human mandible bone is of lesser importance to the applied load [21]. Araldite CY–230 and Hardener HY–951(Araldite, Petro Araldite Private Limited, Chennai, Tamil Nadu) mixture was used in the ratio of 10:1 to prepare a photoelastic block [22] shown in Fig. 4(a).

4.3. Photoelastic disc calibration

A key parameter in Photoelastic analysis is the determination of the fringe constant for the birefringent material being used. Although the material fringe value was specified by the manufacturer, it was necessary to calibrate the material at the time of experimentation as specified in most of the literature [19]. A calibration disc was use from the same batch of acrylic material as the equivalent photoelastic model and the disc calibration was performed with the same light source to calculate photoelastic material fringe constant [20]. Three photoelastic block model for each implant prosthesis is prepared for photoelastic stress analysis.

4.4. Crown fitment in photoelastic block model

Firstly, the implant and abutment are fitted in an acrylic block model (Fig. 4 b). Crown is a replica of missing tooth cemented on the outer surface of abutment. For the implant prostheses, the pattern of wax was used for the suitable shape of a porcelain metal framework. Later, the crowns were relocated, and the efficient interproximal contacts were checked according to clinically adopt procedures. The crown model demonstrates the shape of molar tooth is used for the implant system. The abutment with the crown fitment model is shown in Fig. 4 (c).

4.5. Experimental procedure

The photoelastic block model with implant prosthesis (Fig. 3 (b)) was placed in circular polariscope and the first picture captured without any load, to confirm the block model was stress free. [23] then the vertical occlusal loads of 100 N were employed to pre-determined points on the crowns with an S-type beam load cell. The monochromatic fringe pattern images (Fig. 3(c)) were recorded by a digital camera (Nikon D5200 Digital SLR camera) and later analyses to count the number of fringes (N) using image software (Adobe Photoshop CS6). The photographs were taken from each loading conditions to assess the number of fringes at the point of interest. Fringes were counted at six location (Proximal-Top most portion of implant-bone interface, Mesial-Middle portion at the interface and Distal-bottom portion of implant interface) along left and right side of the implant on photoelastic block model [24], in accordance to a qualitative analysis by some of the researchers. [25,26] The fractional fringes (N1 and N2) is determined by Tardy's method of compensation by rotating analyzer clockwise and anticlockwise direction and the average fringes is calculated as presented in Table 3 (for Type III implant system). All the photographic images obtained from each loading conditions were evaluated to calculate the number of fringes in an isochromatic light source. Optical axes of photoelastic model coincide with principal stress direction due to birefringence effect [27] and the magnitude of principle stress difference (stress intensity in MPa) was calculated using stress optic law with the following relation,

Please cite this article as: P. Dhatrak, U. Shirsat, S. Sumanth et al., Numerical investigation on stress intensity around Bone-Implant interface by 3-Dimensional FEA and experimental verification by optical technique, Materials Today: Proceedings, https://doi.org/10.1016/j.matpr.2020.06.097

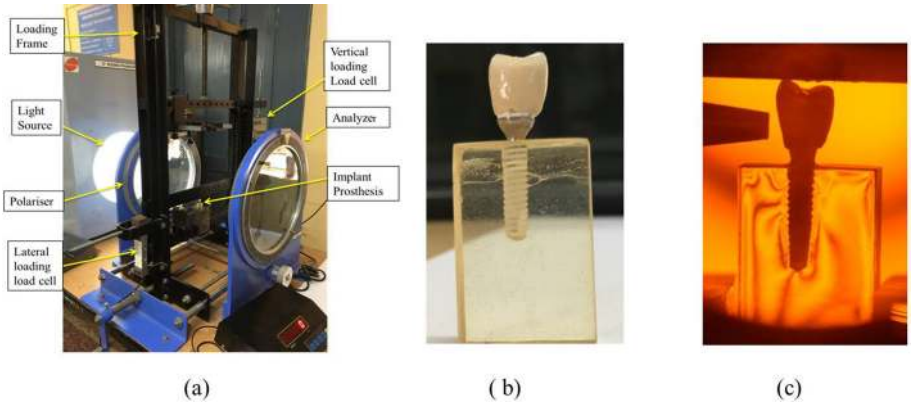

Fig. 3. (a) Photoelastic experimental setup with quarter wave plates (b) Acrylic block model with implant prosthesis (c) Fringe pattern observed under monochromatic light for vertical loading.

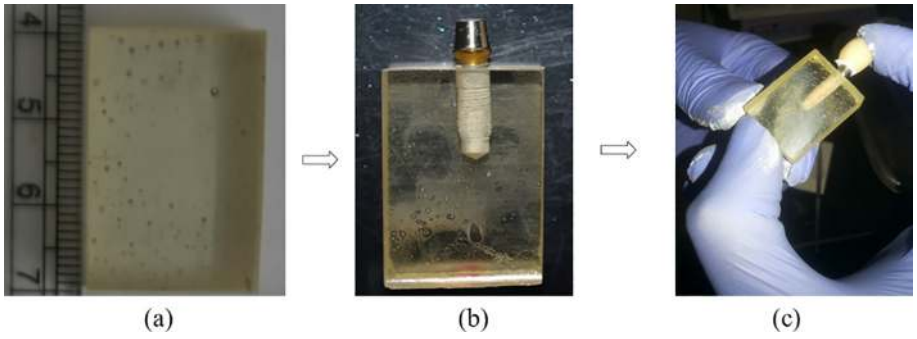

Fig. 4. (a) Acrylic block model (b) Implant and Abutment fitted in the block model (c) Acrylic block model with crown.

Stress Intensity $(\sigma_1\text{-}\sigma_2) = (N f)/h$

Where $\sigma_1$and σ_2 are the principle stresses (MPa), 'N' is the number of fringes found from experimental fringe pattern, 'h' assumed to be the thickness of photoelastic block (mm) and 'f' is the fringe material constant (N/mm per fringe) depends on wavelength of light 'λ' and stress optic coefficient C ($f=\lambda/C$) [19,20].

5. Results and discussions

5.1. Experimental results

Experimental work needs to carry out to accept or reject the hypothesis. In the present research work, it was hypothesized that three photoelastic block model of each implant system differ significantly in their mechanical behavior (stress intensity and stress distribution pattern) at the bone–implant interface. The level of statistical significance is often used as p-value. No significant differences were found in three photoelastic model of each implant prosthesis ($p < 0.05$) based on statistical analysis [28]. Hence the null hypothesis is rejected. Fringe orders and the propagation of stresses along the interface were observed by qualitative analysis and the stress intensity results were obtained by quantitative analysis [17]. The stress is localized and quantify based on the number of fringes calculated. More the number of fringes, more will be the stress intensity; stress concentration will be more as the number of fringes closer to each other [19,20]. We detected a maximum number of fringes in Type-I implant system compared with other four implant system and the stress concentration was greater at the apical section (Near the first thread of implant) for lateral as well as oblique loading in comparison with five-implant system. Minimum number of fringes observed under vertical load and maximum number of fringes under oblique load in Type III implant system presented in Table 3. The fringes were uniformly distributed in Type-III implant system, indicating a lower stress concentration compared with other Implant system.

The greatest stress concentrations were detected at distal region (Near the last thread) under vertical loading whereas at the apical region for the lateral and oblique loading condition for all implant system. In all five type of implant system the maximum stress intensity calculated from experimental analysis.

5.2. Finite element results

The stress intensity in the cancellous bone by FE simulation for Type-III implant system under three loading conditions is shown in Fig. 5. The stress distribution pattern is uniform in Type-III implant system. In vertical loading condition Type- IV shows minimum stress intensity as shown in Fig. 6 whereas for lateral and oblique loading conditions Type-III implant system shows minimum stress intensity (Fig. 7 and Fig. 8). Stress intensity in cancellous bone is found to be more significant to the applied oblique loading condition.

5.3. Experimental and numerical result comparison

Experimental and FEA stress intensity results comparison are presented in Figs. 6, 7 and 8. For Type-II, III and IV implant system, the stress intensity values obtained from FEA are found in approximate close agreement with those calculated from experimental photoelastic analysis under lateral, vertical and oblique loading respectively. Whereas for vertical and lateral loading condition Type-V implant system shows maximum difference as compared

Please cite this article as: P. Dhatrak, U. Shirsat, S. Sumanth et al., Numerical investigation on stress intensity around Bone-Implant interface by 3-Dimensional FEA and experimental verification by optical technique, Materials Today: Proceedings, https://doi.org/10.1016/j.matpr.2020.06.097

Table 3
Experimental results of Photoelastic fringes observed in Type-III Implant System.

100 N Vertical					
Stress Locations	Fringe order	N_1	N_2	N_{avg} (N/mm per fringe)	Stress Intensity (MPa)
Proximal Left P (L)	2	2.33	1.33	1.83	1.47
Proximal Right P (R)	6	5.61	4.22	4.92	3.95
Mesial Left M (L)	4	4.47	3.61	4.04	3.25
Mesial Right M (R)	6	6.55	5.61	6.08	4.89
Distal Left D (L)	7	7.37	6.83	7.10	5.70
Distal Right D (R)	6	6.27	5.55	5.91	4.75
40 N Lateral					
Stress Locations	Fringe order	N_1	N_2	N_{avg} (N/mm per fringe)	Stress Intensity (MPa)
Proximal Left P (L)	5	5.33	4.72	5.03	4.04
Proximal Right P (R)	8	8.38	7.50	7.94	6.38
Mesial Left M (L)	6	6.78	5.78	6.28	5.05
Mesial Right M (R)	6	6.33	5.33	5.83	4.68
Distal Left D (L)	7	7.55	6.55	7.05	5.66
Distal Right D (R)	6	6.55	5.55	6.05	4.86
100 N Oblique 45°					
Stress Locations	Fringe order	N_1	N_2	N_{avg} (N/mm per fringe)	Stress Intensity (MPa)
Proximal Left P (L)	10	10.66	9.61	10.14	8.14
Proximal Right P (R)	11	11.2	10.77	10.99	8.83
Mesial Left M (L)	6	6.50	5.58	6.04	4.85
Mesial Right M (R)	9	9.60	8.68	9.14	7.34
Distal Left D (L)	9	9.34	8.38	8.86	7.12
Distal Right D (R)	9	9.72	8.72	9.22	7.41

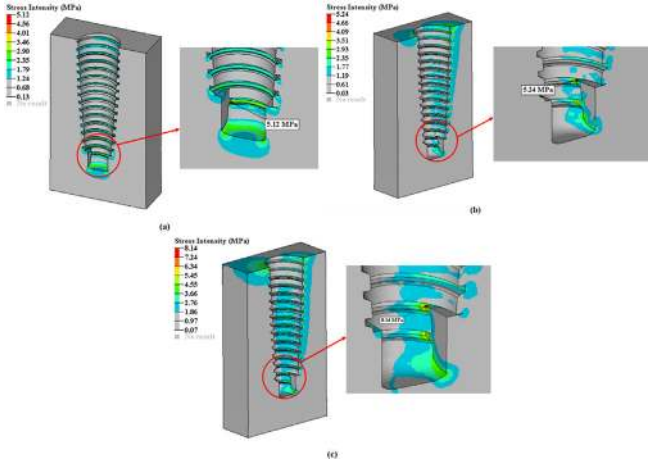

Fig. 5. Cut section of cancellous bone showing stress intensity distribution at the interface region for the implant Type-III system under (a) vertical load (b) Lateral load and (c) 100 N oblique load at 45°.

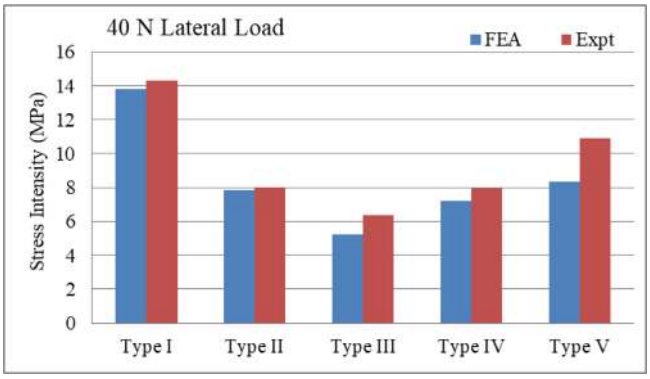

Fig. 7. Experimental and FEA stress intensity result comparison (40 N Lateral load).

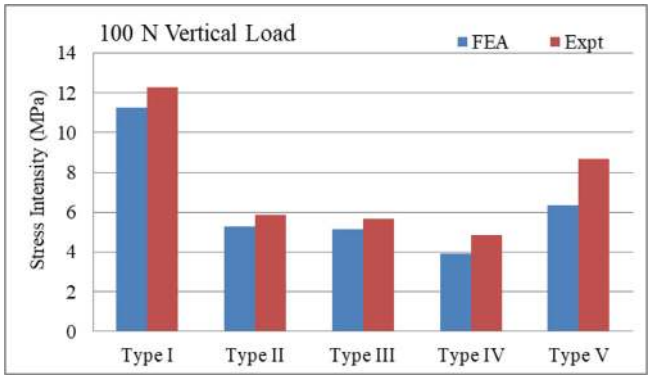

Fig. 6. Experimental and FEA stress intensity result comparison (100 N occlusal load).

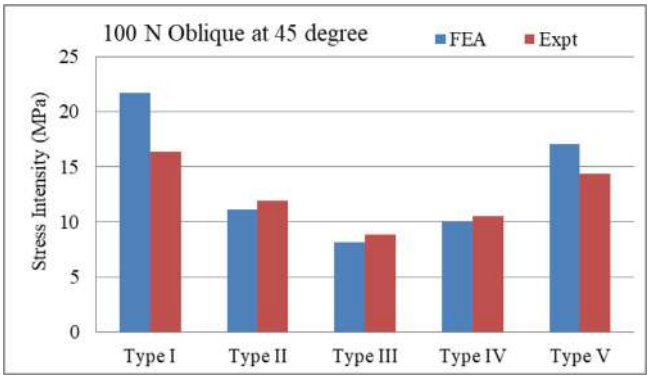

Fig. 8. Experimental and FEA stress intensity result comparison (Oblique 100 N at 45° load).

Please cite this article as: P. Dhatrak, U. Shirsat, S. Sumanth et al., Numerical investigation on stress intensity around Bone-Implant interface by 3-Dimensional FEA and experimental verification by optical technique, Materials Today: Proceedings, https://doi.org/10.1016/j.matpr.2020.06.097

with other implant systems. Correspondingly for oblique loading condition Type-I and Type-V implant system shows the maximum variation in both experimental and FEA results.

This study also addressing some of the limitations and future scope. For an accurate measurement of stress intensity along the interface, the actual shape of bone geometry needs to be simulated in FE study which might decrease the variation between simulated and experimental results. Whereas, in experimentational work, the fringes could be accurately measures using 3D photoelastic technique that needs to be considered in future investigations.

6. Conclusions

Current study compared the stress intensity results obtained from optical technique with those simulated from finite element analysis. Within the limitation of present work, five different commercial implant systems were analyzed using orthotropic material properties of jawbone in numerical simulation. Stress distribution along bone-implant interface shows region of high stress concentration for different loading conditions. Stresses are more concentrated near the interface. Furthermore, the magnitude of stress intensity decreases towards the outer region (away from interface). Based on experimental and numerical analysis results the following inferences can be drawn

1. The critical intensity of stress location was noted at the proximal section for the lateral and oblique loading conditions, whereas for vertical occlusal loading it was in distal region of the interface. The oblique loading (Simulated as real masticatory loads) induces greater stress at the interface as compared with vertical (occlusal load) and lateral loading conditions.
2. Numerical simulation results show that, the use of orthotropic properties for implant prosthetic model is more appropriate than the isotropic for predicting stress intensity along the bone interface.
3. In most of the commercial dental implant systems, cutting flutes regions is found to be region of maximum stress concentration. Also, in some implant systems, uneven distribution of stress was observed at the interface. Type-III and Type-IV implant showed uniform stress distribution along the length of implant for all loading condition. Therefore, uniform stress distribution ultimately gives better stability which leads to increase the success rate.
4. The thread profile of the implants is one of the critical parameters to effectively distribute the stress intensity and avoid high stress concentration at cancellous bone near the interface.

CRediT authorship contribution statement

Pankaj Dhatrak: Conceptualization, Data curation, Formal analysis, Funding acquisition, Investigation, Methodology, Software, Validation, Visualization, Writing - original draft. **Uddhav Shirsat:** Data curation, Investigation, Project administration, Supervision, Validation, Visualization, Writing - review & editing. **S. Sumanth:** Methodology, Validation, Visualization, Writing - review & editing. **Vijay Deshmukh:** Methodology, Validation, Visualization.

Declaration of Competing Interest

The authors declare that they have no known competing financial interests or personal relationships that could have appeared to influence the work reported in this paper.

Acknowledgments

This research work was sponsored by Savitribai Phule Pune University (BCUD), Pune (BCUD Online Proposal No. 13ENG001550, BCUD: Fin/Bill/2013-14/1984-6) and supported by M. A. Rangoonwala College of Dental Science and Research Centre, Pune, India.

References

[1] S. Faegh, S. Muftu, Load transfer along the bone–dental implant interface, J. Biomech. 43 (2010) 1761–1770.
[2] P. Ausiello, P. Franciosa, M. Martorelli, David C. Watts, Effects of thread features in Osseo-integrated titanium implants using a statistics-based finite element method, Dental Mater. 28 (2012) 919–927.
[3] J. Chen, Z. Zhang, X. Chen, C. Zhang, G. Zhang, X.u. Zhewu, Design and manufacture of customized dental implants by using reverse engineering and selective laser melting technology, J. Prosthetic Dentistry 112 (2014) 1088–1095.
[4] T. Li, K. Hub, L. Cheng, Y. Ding, Y. Ding, J. Shao, L. Kong, Optimum selection of the dental implant diameter and length in the posterior mandible with poor bone quality – A 3D finite element analysis, Appl. Math. Model. 35 (2011) 446–456.
[5] Marcelo Bighetti Toniollo, Ana Paula Macedo, Renata Cristina Silveira Rodrigues, Ricardo Faria Ribeiro PhD3, Maria da Gloria Chiarello de Mattos PhD, 'A three-dimensional finite element analysis of the stress distribution on morse taper implants surface' Journal of Prosthodontic Research (2013).
[6] U. Lekholm, G.A. Zarb, Patient Selection and preparation. Tissue integrated prostheses: osseointegration in clinical dentistry. Quitssence Publishing Company, Chicago, USA (1985) 199-209.
[7] B. Piotrowski, A.A. Baptista, E. Patoor, P. Bravetti, A. Eberhardt, P. Laheurte, Interaction of bone-dental implant with new ultra-low modulus alloy using a numerical approach, Mater. Sci. Eng. C 38 (2014) 151–160.
[8] Lu. Songhe, Tao Li, Yongqiang Zhang, Lu. Chunlei, Yingying Sun, Biomechanical optimization of the diameter of distraction screw in distraction implant by three-dimensional finite element analysis, Comput. Biol. Med. 43 (2013) 1949–1954.
[9] Vincent Mathieu, Romain Vayron, Gilles Richard, Gregory Lambert, Salah Naili, Jean-Paul Maningaud, Guillaume Haiat, Biomechanical determinants of the stability of dental implants: Influence of the bone-implant interface properties, J. Biomech. 47 (2014) 3–13.
[10] Shih-Hao Chang, Chun-Li Lin, Shue-Sang Hsue, Yang-Sung Lin, Shiang-Rung Huang, Biomechanical analysis of the effects of implant diameter and bone quality in short implants placed in the atrophic posterior maxilla, Med. Eng. Phys. 34 (2012) 153–160.
[11] Jan Wolff, Nathaniel Narra, Anna-Kaisa Antalainen, Jiri Valasek, Jozef Kaiser, George K. Sandor, Petr Marcian, Finite element analysis of bone loss around failing implants, Mater. Des. 61 (2014) 177–184.
[12] Pankaj Dhatrak, Vedant Girme, Uddhav Shirsat, S. Sumanth, Vijay Deshmukh, Significance of orthotropic material models to predict stress around bone-implant interface using numerical simulation, BioNanoScience (2019), https://doi.org/10.1007/s12668-019-00649-5.
[13] S.H. Chang, S.R. Huang, S.F. Huang, C.L. Lin, Mechanical response comparison in an implant overdenture retained by ball attachments on conventional regular and mini dental implants: a finite element analysis, Computer Methods Biomech. Biomed. Eng. 19 (2015) 911–921.
[14] ABAQUS/CAE Analysis Manual, Documentation V6.13, Simulia Dassault Systems, RI, USA, (2007).
[15] K. Verplancke, W. De Waele and H. De Bruyn, Dental Implants, what should be known before starting an In-Vitro study, Sustainable Construction and Design by Laboratory Soete, 2011?.
[16] I. Hasan, B. Roger, F. Heinemann, L. Keilig, C. Bourauel, Influence of abutment design on the success of immediately loaded dental implants: Experimental and numerical studies, Med. Eng. Phys. 34 (2010) 817–825.
[17] Eduardo Piza Pellizzer, Caroline Cantieri de Mello, Joel Ferreira Santiago Junior, Victor Eduardo de Souza Batista, Daniel Augusto de Faria Almeida, Fellippo Ramos Verri, Analysis of the biomechanical behavior of short implants: The photo-elasticity method, Materials Science and Engineering C 55 (2015) 187–192.
[18] F. Lofaj, J. Kucera, D. Nemeth, L. Kvetkova, Finite element analysis of stress distributions in mono- and bi-cortical dental implants, Mater. Sci. Eng., C 50 (2015) 85–96.
[19] Doyle JF, Phillips JW Manual on experimental stress analysis 5th ed. Society for Experimental Mechanics (U.S.) 1989.
[20] J.W. Dally, F.W. Riley, Experimental Stress Analysis, McGraw-Hill Inc, 1991.
[21] Hao-Sheng Chang, Yi-Chin Chen, Yao-Dung Hsieh, Ming-Lun Hsu, Stress distribution of two commercial dental implant systems: A three-dimensional finite element analysis, J. Dental Sci. 8 (2013) 261–271.
[22] K. Ramesh, M.P. Hariprasad, S. Bhuvanewari, Digital photoelastic analysis applied to implant dentistry, Opt. Lasers Eng. 87 (2016) 204–213.
[23] Marcelo Coelho Goiato, Aldieris Alves Pesqueira, Daniela Micheline Dos Santos, Macela Filie Haddad, Amalia Moreno, Photoelastic stress analysis in prothetic

implants of different diameters: Mini, narrow, standard or wide, J. Clin. Diagn. Res. 8 (9) (2014) ZC86–ZC90.

[24] Pankaj Dhatrak, Uddhav Shirsat, S. Sumanth, Vijay Deshmukh, Finite element analysis and experimental investigations on stress distribution of dental implants around implant-bone interface, Mater. Today: Proc. 5 (2018) 5641–5648.

[25] E.P. Pellizzer, R.I. Carli, R.M. Falcon-Antenucci, F.R. Verri, M.C. Goiato, L.M. Villa, Photoelastic analysis of stress distribution with different implant systems, J. Oral Implantol. 40 (2014) 117–122.

[26] B.P. Tonella, E.P. Pellizzer, R.M. Falcon-Antenucci, R. Ferraco, D.A. de Faria Almeida, Photoelastic analysis of biomechanical behavior of single and multiple fixed partial prostheses with different prosthetic connections, J. Craniofac. Surg. 22 (2011) 2060–2063.

[27] Izabella P. Pereira, Rafael L.X. Consani, Marcelo F. Mesquita, Mauro A.A. Nóbilo, Photoelastic analysis of stresses transmitted by complete dentures lined with hard or soft liners, Mater. Sci. Eng., C 55 (2015) 181–186, https://doi.org/10.1016/j.msec.2015.05.020.

[28] Rodrigo Tiossi, Marco A.A., Vasco, Lianshan Lin, Heather J. Conrad, Osvaldo L. Bezzon, Ricrdo F. Ribeiro, Alex S. L. Fok, Validation of finite element models for strain analysis of implant-supported protheses using digital image correlation, Dental Materials 29 (2013) 788-796.

Please cite this article as: P. Dhatrak, U. Shirsat, S. Sumanth et al., Numerical investigation on stress intensity around Bone-Implant interface by 3-Dimensional FEA and experimental verification by optical technique, Materials Today: Proceedings, https://doi.org/10.1016/j.matpr.2020.06.097